Ocean Dynamics
DOI 10.1007/s10236-013-0662-9

Man-induced regime shifts in small estuaries—I: theory

Johan C. Winterwerp · Zheng Bing Wang

Received: 21 February 2013 / Accepted: 15 October 2013

Abstract This is Part I of two papers on man-induced regime shifts in small, narrow, and converging estuaries, with focus on the interaction between effective hydraulic drag, fine sediment import, and tidal amplification, induced by river engineering works, e.g., narrowing and deepening. In this part, a simple linear analytical model is derived, solving the linearized shallow water equations in exponentially converging tidal rivers. Distinguishing reflecting and non-reflecting conditions, a non-dimensional dispersion equation is derived which yields the real and imaginary wave numbers as a function of the estuarine convergence number and effective hydraulic drag. The estuarine convergence number describes the major geometrical features of a tidal river, e.g., intertidal area, convergence length, and water depth. This model is used in Part II analyzing the historical development of the tide in four rivers. Part I also presents a conceptual model on the response of tidal rivers to narrowing and deepening. It is argued that, upon the loss of intertidal area, flood-dominant conditions prevail, upon which fine sediments are pumped into the river, reducing its effective hydraulic drag. Then a snowball effect may be initiated, bringing the river into a hyper-turbid state. This state is self-maintaining because of entrainment processes, and favorable from an energetic point of view, and therefore highly stable. We may refer to an alternative steady state.

Responsible Editor: Rockwell Geyer

This article is part of the Topical Collection on *Physics of Estuaries and Coastal Seas 2012*

J. C. Winterwerp (✉) · Z. B. Wang
Deltares (formerly WL|Delft Hydraulics), PO Box, 177,
2600 MH Delft, The Netherlands
e-mail: han.winterwerp@deltares.nl

J. C. Winterwerp · Z. B. Wang
Environmental Fluid Mechanics, Delft University of Technology,
PO Box 5048, 2600 GA Delft, The Netherlands

Published online: 12 November 2013

Keywords Tidal amplification · Hydraulic drag · Dispersion equation · Regime shift · Elbe · Ems · Loire · Scheldt

1 Introduction

Figure 1 depicts the evolution of the tidal range over roughly the last century in five European ports, which are all situated more than 50 km from the mouth of fairly small and narrow estuaries. It is generally accepted that this large tidal amplification is caused by the ongoing deepening and canalization of these rivers, accommodating ever-larger ships; though the precise mechanisms behind are not yet understood. Of course, the increases in high water levels, and decreases in low water levels form serious problems by themselves, e.g., enhanced flood levels, lowering of ground water table. However, it becomes more and more evident that such deepening and narrowing induce large environmental problems as well. Infamous are the Ems (Germany) and Loire (France) Rivers. Today, both rivers can be characterized as hyper-turbid, with suspended sediment (suspended particulate matter (SPM)) concentrations of several 10 g/l, and large-scale occurrences of fluid mud. Strong vertical stratification causes serious water quality problems, and in the Loire the enhanced salinity intrusion hampers fresh water intake for industry and agriculture. The causes of the evolution of Loire and Ems to these hyper-turbid states are not yet fully understood (Talke et al 2008, 2009; Chernetsky et al 2010; Winterwerp 2011), though there is consensus that the large amplification of the tidal range must have played an important role.

The aim of this paper is to enhance our understanding on the evolution of the tidal amplification in narrow estuaries in general, and the evolution towards a hyper-turbid state in particular. This is done by analyzing the historical developments of the tide in four rivers, e.g., the Elbe, Ems,

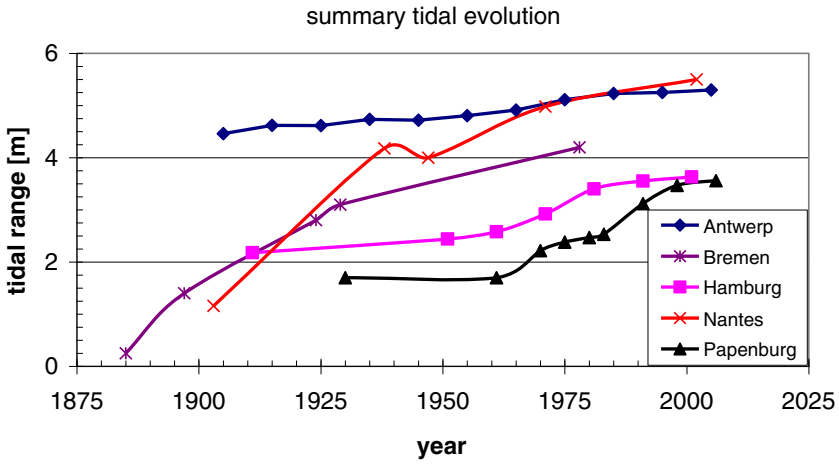

Fig. 1 Tidal evolution in five European ports (Antwerp along Scheldt, Belgium; Bremen along Weser, Germany; Hamburg along Elbe, Germany; Nantes along Loire, France; and Papenburg along Ems, Germany)

Loire, and Scheldt (the only rivers for which sufficient detailed data are available). Part II of this paper describes the results of this analysis, which is carried out using the simple analytical model of the tidal propagation in narrow tidal rivers, described in the present Part I of this paper.

The model presented here is certainly not the first analytical approach of the water movement equations. In fact, analytical studies on the behavior of tides in estuaries go back many decades. Hunt (1964) was probably the first to emphasize the important role of channel convergence on tidal propagation—all estuaries treated in the present paper have a converging plan form. However, the first complete description is most likely by Dronkers (1964). Since his pioneering work, many more studies have been published on the analytical solutions of the shallow water equations in estuaries. LeBlond (1978) analyzed the tidal propagation and phase speed in the Frazer and Saint Lawrence Rivers, which were schematized as straight channels with a rectangular cross-section. When the friction length is small compared to the tidal wave length, i.e., when friction dominates, the wave equations become diffusive, explaining the observed tidal propagation in these two rivers.

Prandle and Rahman (1980) pursued a systematic study on the effects of channel convergence on tidal propagation in general, and on tidal amplification in response to reflections against a barrier in particular. The channel convergence was modeled through power law functions of both river depth and width, and the friction term was linearized, as in the current study. Through a series of diagrams, the role of estuarine parameters on tidal amplification, such as length, location of the barrier, etc. was studied.

Jay (1991) generalized the solutions even further by studying the tidal wave propagation in channels with converging topography, accounting for intertidal areas, river flow, and reflections and including first-order non-linear effects with respect to tidal amplitude, advection, and friction. From his general solutions, Jay established three regimes. The first two regimes are characterized by small friction effects, and are described by the "standard solution" of Green's model. These regimes are referred to as weakly dissipative (Lanzoni and Seminara 1998). The first regime is governed by strong topographic effects (strong convergence of the estuary), and in the second regime, acceleration effects dominate. When topographic and acceleration effects balance, friction becomes progressively more important, and Jay refers to "critical conditions" (e.g., strongly dissipative, Lanzoni and Seminara 1998). The wave equations become parabolic, and diffusive in character, contrary to the hyperbolic behavior of frictionless systems.

The effects of channel convergence in rivers with intertidal area were further studied by Friedrichs and Aubrey (1994), a priori assuming that horizontal velocity gradients are small. This assumption was verified for three tidal rivers, e.g., the Delaware, the Thames, and the Tamar River. Such conditions are referred to as synchronous, and we will see later in the current paper that these are important in understanding the response of tidal rivers to ongoing deepening. In that case, the water movement equations simplify considerably, revealing a 90° phase difference between water level and tidal flow. The tide in such synchronous estuaries is not a classical standing wave, as emphasized by many authors. Friedrichs and Aubrey further introduce a proxy for the tidal asymmetry, referred to as γ, which is the ratio of the wave celerity at high and low water. For $\gamma > 1$, the tide is flood-dominant, which was verified for the three rivers above. An excellent summary of this work is given in Friedrichs (2010), presenting approximations of tidal characteristics in estuaries of a wide variety in shapes and bathymetries.

Lanzoni and Seminara (1998) also study the complete, non-linear water movement equations, distinguishing four estuarine regimes, identified by weak and strong dissipation and weak and strong convergence, respectively. Further to this distinction, the water movement equations are scaled in different ways, yielding four different solutions. One

conclusion, relevant for the current study, is that for strongly dissipative systems, ebb-dominant conditions would prevail, whereas in weakly dissipative estuaries, the tide is always flood dominant.

Toffolon and Savenije (2011) summarize the work by Savenije (2001) and Toffolon et al. (2006), presenting a complete solution of the linearized water movement equations for narrow estuaries with intertidal area, including the effects of limited length (reflections against a weir). They introduce an iterative procedure accounting for the non-linear effects of friction and relatively large tidal amplitude. In case of a closed-end estuary with non-constant depth, the estuary is divided in sub-sections, and a set of linear equations is obtained with internal boundary conditions at the junction of these sub-sections. Cai et al. (2012) elaborate further on this work by analyzing the effects of a somewhat different friction model.

The model by Van Rijn (2011) is basically similar to that of Toffolon and Savenije (2011), though Van Rijn followed a somewhat different approach. Further to these linear analyses, followed by most authors, Van Rijn also elaborates an energy approach in which non-linearities are explicitly accounted for, at the cost though of unknown values of phase angle and flow velocity, which have to be derived from the linear model.

All these studies elaborate more or less on the linearized water movement equations. However, for (fine) sediment transport, tidal asymmetry may be an even more important parameter, which however can only be studied when non-linear effects in the equations are accounted for. This has been done for instance by Jay (1991—though with very little emphasis), Lanzoni and Siminara (1998), Talke et al. (2008), Talke et al. (2009), Chernetsky et al. (2010), and Schuttelaars et al. (2012), by maintaining first- and/or second-order non-linearities in their equations. Speer and Aubrey (1985) and Friedrichs and Aubrey (1988) presented numerical solutions of the water movement equations for an idealized, shallow, and long estuary with a non-converging channel and constant, rectangular cross-section, but including the non-linear advection and friction terms, and the effects of intertidal area. The results were presented in a series of famous diagrams, indicating when ebb- or flood-dominancy can be expected as a function of the tidal amplitude relative to the water depth, and areal of intertidal area.

In the current papers, we study the evolution of the tide and SPM concentrations in narrow estuaries with intertidal area, and possibly of limited length (weir) in response to human interventions, e.g., narrowing and deepening by analyzing observed changes in tidal properties. For this purpose we need a simple and transparent model, allowing comparison of the various rivers under consideration, focusing on tidal damping/amplification mainly. The analytical models summarized above are either complete, but not too transparent, or are based on simplifications which prohibit application over the full range of conditions considered in the present papers. Therefore, we derive an alternative solution, which is basically identical to the work by Jay (1991), Toffolon and Savenije (2011), and Van Rijn (2011), but contains three parameters only. This model is derived in Section 4, and then applied to analyze the response of an estuary to narrowing and deepening conceptually in Section 5.

A crucial step in our analysis is the influence of suspended matter (fine sediments) on the effective hydraulic drag in (tidal) rivers, as a result of which the response of a river to narrowing and deepening becomes amplified, as explained in Section 2. This amplification may become so large that the river develops an alternative steady state—the hyper-turbid regime. We refer to a regime shift, which is elaborated upon in the Sections 3 and 6.

In Part II of this paper, the conceptual picture described in the current Part I is applied to the Elbe, Ems, Loire, and Scheldt rivers. Historical data on river engineering works and the tidal response to these interventions are analyzed with the analytical model of Part I, discussing the effects of SPM on the effective hydraulic drag, and the effects of tidal reflections against constructions in the river.

2 Suspended matter and effective hydraulic drag

In this paper, the effective hydraulic drag in a tidal river is expressed in terms of the Chézy coefficient C, as C relates directly to the logarithmic law of the wall, and we can use $U/u_* = C/\sqrt{g}$, where U=depth−mean flow velocity, u_*=shear velocity, and g=gravitational acceleration. When deepening a river by, e.g., dredging, the effective hydraulic drag is known to be affected in two ways, i.e., by the increase in depth itself, where the bed structure (roughness height k_s) remains unchanged, and by off-topping possible bed forms in the river. This can easily be seen from the relation between C and k_s:

$$C = 18\log\{12h/k_s\} \tag{1}$$

This relation shows that when the water depth is doubled at constant k_s, C increases by at most 5 $m^{1/2}/s$.

Van Rijn (1993) shows that by reducing bed form heights in tidal rivers, k_s may decrease by a decimeter or so. In that case, Eq. 1 shows that again C may increase by about another 5 $m^{1/2}/s$. We show in Part II that such a decrease in bed forms may have taken place in for instance the Elbe River.

However, there is a third mechanism that may reduce the effective hydraulic drag, i.e., stratification effects by suspended matter (Vanoni 1946; Taylor and Dyer 1977; Soulsby and Wrainwright, 1987; Villaret and Trowbridge 1991, to name a few). Vertical stratification by suspended matter reduces the vertical exchange of turbulent momentum, reducing viscous dissipation. In case of fine suspended

sediments, these stratification effects are well distributed over the water column (e.g., Soulsby and Wainwright 1987), and therefore quite effective. Winterwerp et al. (2009) proposed a simple formula for the reduction in hydraulic drag, induced by suspended matter:

$$\frac{\overline{u}}{u_*} \equiv \frac{C_{\mathrm{eff}}}{\sqrt{g}} = \frac{C_0}{\sqrt{g}} + \frac{C_{\mathrm{SPM}}}{\sqrt{g}} = \frac{C_0}{\sqrt{g}} + 4h\mathbf{Ri}_*\beta \tag{2}$$

where C_0 and C_{SPM} are the Chezy values for sediment-free conditions, and for the sediment-induced effects, respectively with the bulk Richardson number $\mathbf{Ri}_*$ and Rouse number β defined as:

$$\mathbf{Ri}_* \equiv \frac{(\rho_b - \rho_w)gh}{\rho_b u_*^2} \quad \text{and} \quad \beta \equiv \frac{\sigma_T W_s}{\kappa u_*} \tag{3}$$

where ρ_b and ρ_w are the bulk density of the suspension and clear water, respectively, W_s=the effective settling velocity, σ_T=Prandtl-Schmidt number (~0.7–1), and κ=von Kármàn constant (~0.4). Relation (2) is depicted in Fig. 2 (after Winterwerp et al. 2009); the various "data points" reflect the results of a large number of numerical simulations.

With increasing SPM concentrations, $\mathbf{Ri}_*$ increases, whereas for larger particles (flocs), β increases. Basically, Fig. 2 depicts that with increasing SPM concentrations, C_{eff} increases. For the rivers under consideration in Part II, water depths vary between 5 and 10 m, though the Elbe is considerably deeper. In that case, Chézy values may increase by 15–30 $m^{1/2}/s$, considerably more than for the two other mechanisms. It is to be noted that such effects may occur at SPM concentrations as low as several 100 mg/l, provided that these elevated concentrations are found over a substantial length of the river (Winterwerp et al. 2009). In the following, it is hypothesized how this interaction between suspended matter and turbulent flow may initiate a snowball effect, leading to the regime shifts observed in, e.g., the Ems and Loire Rivers.

3 A second estuarine turbidity maximum—the hyper-turbid state

Most estuaries are characterized by elevated SPM concentrations at the head of the salinity intrusion. This phenomenon is known as the estuary turbidity maximum (ETM). All textbooks on estuarine dynamics explain the mechanisms behind the occurrence of such ETM (e.g., Dyer 1997), and the general consensus is that this ETM is largely governed by a balance between river-induced flushing and up-estuary transport by estuarine circulation (also known as gravitational circulation). Other, often secondary processes contributing to the dynamics of an ETM are Stokes' drift and its rectification, tidal asymmetry effects, and lag effects (scour and settling lag). In the following we refer to this turbidity maximum found at the head of salinity intrusion as ETM1.

However, under special conditions, processes other than the estuarine circulation may dominate the ETM dynamics, in which case no correlation with salinity intrusion is found. For instance, Brenon and LeHir (1999) studied the processes on the formation of the turbidity maximum in the Seine estuary with the use of a three-dimensional model, comparing model output with observations. From a sensitivity analysis they concluded that in the Seine, the estuarine turbidity maximum at spring is mainly governed by a process referred to as tidal pumping, e.g., the asymmetry in peak tidal velocities.

Lin and Kuo (2001) carried out field measurements in the York River (USA) and found a second ETM, beyond the salinity-driven ETM1. Lin and Kuo argued that this ETM is maintained by tidal asymmetry and lag effects, in conjunction with a large availability of fine sediments in the riverbed.

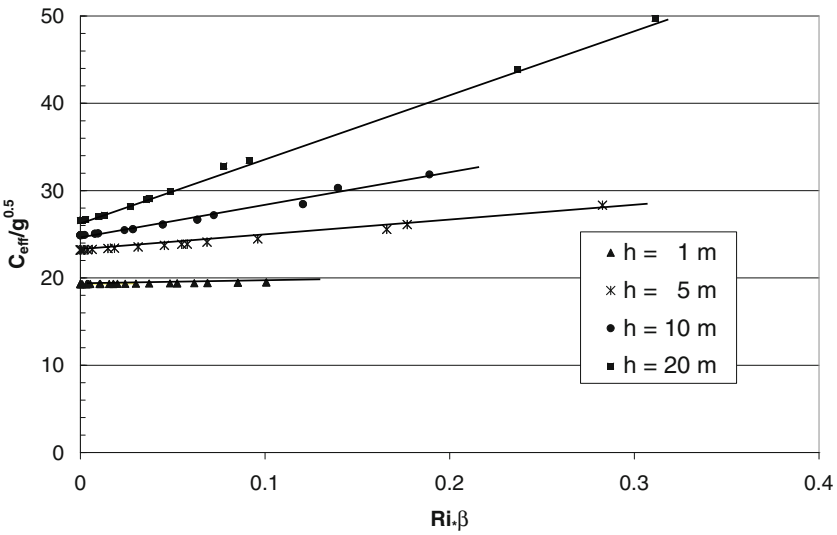

Fig. 2 Increase in effective Chézy coefficient as a function of Richardson and Rouse number, and water depth, based on the semi-analytical approach by Winterwerp et al. (2009)

Chernetsky et al. (2010) discussed the formation of a secondary ETM in the Ems River, well beyond the area of salinity intrusion, which is clearly depicted in Talke et al. (2009). The dynamics of this ETM are governed by tidal asymmetry, in response to ongoing deepening of the river. We refer to this second turbidity maximum as ETM2, and for simplicity in the following argumentations, we define:

- ETM1 is controlled by a balance between river-induced flushing and estuarine circulation
- ETM2 is controlled by a balance between river-induced flushing and asymmetry in peak tidal velocities, in which we are purposely ignoring other effects.

This picture is sketched in Fig. 3, showing conceptually that ETM1 and ETM2 can exist together, and that ETM2 is always found up-estuary of ETM1. However, in practice, ETM1 and ETM2 may merge, as in the Ems (Talke et al. 2009).

Winterwerp (2011) postulated a sequence of developments in estuarine dynamics in response to river deepening through which an ETM2 is formed in rivers which are initially characterized by a regime with one ETM1 only. It was argued that, if SPM concentrations become large enough, a self-maintaining alternative regime would evolve with an ETM2, dominated by asymmetries in peak velocities and vertical mixing (internal asymmetry, e.g., Jay and Musiak 1996), balanced by river-induced flushing.

Hence, a tidal river may be characterized by two alternative steady states, one state (regime) with only one ETM1, and one with an ETM2 (possibly in conjunction with an ETM1 as well). In the following sections, we will argue further how such a regime shift may develop in response to river engineering works. Here we summarize two arguments on the stability of the second regime.

The first argument follows from the stability diagram for suspensions of fine sediments in open channel flow, developed by Winterwerp (2001, 2006, e.g., Fig. 4). The horizontal axis of Fig. 4 depicts the volumetric concentration ϕ of the suspended sediment particles, which, for fine sediments, can be large at small mass concentrations because fine sediment flocs contain large amounts of water. The vertical axis depicts the flux Richardson number $\mathbf{Ri_f}$, a measure for the efficiency of vertical mixing, which can be interpreted as the ratio of potential energy required for mixing

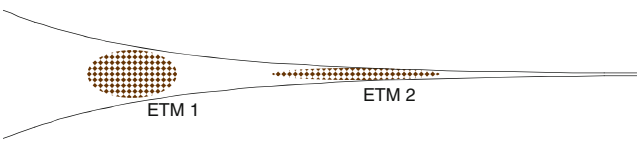

Fig. 3 Cartoon of the turbidity maxima ETM1 and ETM2 in a converging estuary; ETM1 is governed by river-induced flushing and estuarine circulation, whereas ETM2 is governed by river-induced flushing and tidal asymmetry

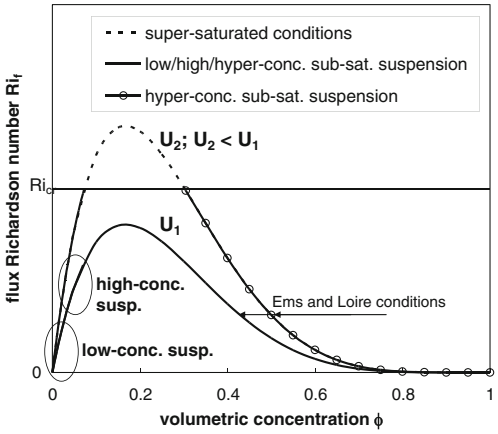

Fig. 4 Stability diagram for fine sediment suspensions showing that a bi-modal behavior—a particular Richardson number can be obtained at two different SPM concentrations (after Winterwerp 2006)

of fine sediments over the water column, and the kinetic energy available for mixing. Experimental evidence shows that a turbulent flow cannot be stable when $\mathbf{Ri_f}$ exceeds a critical value, reflected by $\mathbf{Ri_{f,cr}}$ (e.g., Turner 1973; Winterwerp 2001). Figure 4 shows that at a flow velocity U_2, SPM concentrations may attain values for which $\mathbf{Ri_f} > \mathbf{Ri_{f,cr}}$, upon which the turbulent flow field collapses. In practice, this means that fluid mud is formed.

At larger flow velocity $U_1 > U_2$, the stability curve is continuous, with two distinctly different branches though. In the left, rising branch, an increase in ϕ implies an increase in $\mathbf{Ri_f}$, hence less favorable conditions from an energetic point of view. In the right, descending branch, an increase in ϕ yields a decrease in $\mathbf{Ri_f}$, hence energetically more favorable conditions. This branch refers to so-called hyper-concentrated conditions: the turbulent flow "likes" high concentrations, as a further increase in ϕ requires less energy to keep the sediment in suspension. It can be argued that the Ems and Loire Rivers are currently in this hyper-concentrated state (Winterwerp 2011). The bi-modal behavior of Fig. 4 is attributed to hindered settling effects—at higher ϕ—values, the effective settling velocity reduces, and less energy is required to keep the particles in suspension (e.g., Winterwerp 2001; Dankers and Winterwerp 2007).

It is noted that in case of asymmetries in peak tidal velocity, also vertical mixing becomes asymmetric (mixing scales with velocity squared). For instance, flood conditions may be well-mixed, whereas ebb conditions may be highly stratified (e.g., Winterwerp 2011).

The last important issue on the hyper-concentrated state of tidal rivers concerns the temporal variation in tidal velocity. Around slack water, the suspension settles, forming fluid mud, which then starts to consolidate. So how does the sediment–water mixture remain fluid? Bruens et al. (2012) suggest that during accelerating flow, water overlying the fluid mud is pumped into the fluid mud by entrainment processes. Hence, twice every tidal cycle, the suspension is more or less entirely

mixed over the water column. As consolidation rates scale with the fluid mud thickness squared, consolidation is only important over longer time periods, such as the spring-neap cycle.

In this section, we have argued that when conditions would evolve inducing an ongoing increase in SPM concentrations, a regime shift may occur leading to hyper-concentrated conditions. Such a hyper-turbid regime is extremely stable, as favorable from an energetic point of view. Therefore, a river in this state would be difficult to reverse to its original state, as the "energy barrier" of Fig. 4 has to be overcome (or by-passed).

When the river flow is too small to flush the fine sediments occasionally out of the river, the development of an ETM2 regime is a likely candidate to set a regime shift into motion, as the asymmetries in peak velocity and vertical mixing continue to pump fine sediments up-estuary (or trap riverine sediments). Obviously, also the river's flushing capacity decreases with increasing water depth. In the two following sections, we discuss how engineering works may initiate such events.

4 Dispersion equation for converging estuaries

Basically, all alluvial estuaries have a more or less funnel-shaped plan form. In the remainder, we limit ourselves to the evolution of the semi-diurnal tide ($T \approx 12.5$ h) in narrow estuaries (one channel only) with intertidal area and an exponentially converging width: $b_c = b_0 \exp\{-x/L_b\}$, where b_c=width flow-carrying cross-section, b_0=width flow-carrying cross-section in the mouth of the estuary, and L_b= convergence length (typical values between ~20 and ~40 km). Furthermore, we assume a more or less rectangular shape of the flow-carrying cross-section, such that $A_c \approx h b_c$, where A_c=area of flow-carrying cross-section, and h=tide-mean water depth, and a width of the intertidal area Δb, which is a constant fraction of $b_c(x)$. The total width b_{tot} is the sum of b_c and Δb. This cross-section is sketched in Fig. 5.

This configuration is fairly similar to the ones studied by Jay (1991), Lanzoni and Seminara (1998), Friedrichs and Aubrey (1994), Toffolon and Savenije (2011), and Van Rijn (2011). The governing equations for conservation of mass and momentum have been linearized by neglecting the advection term and linearizing the friction term in the momentum equation (see also references above):

$$\begin{aligned} (b_c + \Delta b)\frac{\partial \eta}{\partial t} + \frac{\partial A_c u}{\partial x} &= 0 \\ \frac{\partial u}{\partial t} + g\frac{\partial \eta}{\partial x} + \frac{ru}{h} &= 0 \end{aligned} \tag{4}$$

where η=instantaneous water level, u=cross-sectional averaged flow velocity, r=linear friction term ($r = 8c_D U/3\pi$ [m/s]), c_D=drag coefficient, U=characteristic (maximal velocity), and x and t are longitudinal co-ordinate and time ($x=0$ at the estuaries mouth, and $x>0$ up-estuary). The drag coefficient c_D attains values of 0.001 to 0.003 (corresponding Chézy values of 100–60 $m^{1/2}/s$, as $r \approx gU/C^2$), hence r also varies from around 0.001 to 0.003. In the following, we assume that the fresh water river flow is so small that its effects can be neglected. Finally, further to our linear approach, we also assume that parameters may vary along the estuary, such as the tidal amplitude, but that these variations are relatively small, and that the tidal amplitude is small compared to the water depth.

If we neglect longitudinal gradients in water depth ($\partial h/\partial x$), the continuity and mass balance equation read:

$$\frac{\partial \eta}{\partial t} + \frac{A_c}{b_c + \Delta b}\frac{\partial u}{\partial x} - \frac{A_c}{b_c + \Delta b}\frac{u}{L_b} = 0 \tag{5a}$$

$$\frac{\partial u}{\partial t} + g\frac{\partial \eta}{\partial x} + \frac{ru}{h} = 0 \tag{5b}$$

We assume that the solution to (5) follows a harmonic function:

$$\eta(x,t) = h + a_0 \exp\{i(\omega t - kx)\} \quad \text{and} \quad u(x,t) = U_0 \exp\{i(\omega t - kx - \varphi)\} \tag{6}$$

where a_0=tidal amplitude at $x=0$ (because of our linear approach, a_0 should be much smaller than the water depth h), U_0=amplitude flow velocity at $x=0$, ω=tidal frequency; $\omega = 2\pi/T$; T=tidal period, k=complex wave number; $k = k_r + ik_i$, k_r=real wave number ($k_r = 2\pi/\lambda$), λ=tidal wave length, k_i=imaginary wave number, and φ=phase angle between tide and velocity. Tidal amplification/damping is then defined as $a(x) = a_0 \exp\{k_i x\}$.

Next, we substitute (6) into (5a) and (5b), which reads in matrix form:

$$\begin{bmatrix} i\omega & -\left(\frac{A_c}{b_c + \Delta b} ik + \frac{A_c}{b_c + \Delta b}\frac{1}{L_b}\right)\exp\{-i\varphi\} \\ igk & -\left(i\omega + \frac{r}{h}\right)\exp\{-i\varphi\} \end{bmatrix} \begin{bmatrix} a_0 \\ U_0 \end{bmatrix} = 0 \tag{7}$$

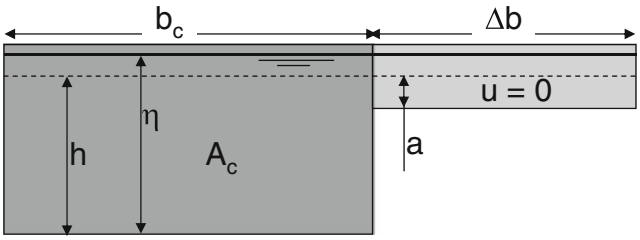

Fig. 5 Schematic cross-section of tidal river with flood plain, and definition of parameters used

Requiring the existence of non-trivial solutions, the determinant of Eq. 7 should be zero, which yields a dispersion equation implicit in the wave number k:

$$L_b k^2 - ik\frac{b_c+\Delta b}{ghb_c}L_b\omega^2\left(1-i\frac{r}{\omega h}\right)=0 \quad \text{or} \quad \kappa^2-2i\kappa-\Lambda_e(1-ir_*)=0 \tag{8}$$

in which the following dimensionless parameters have been defined:

$$\begin{aligned}
\kappa &= \kappa_r + i\kappa_i = 2kL_b \\
L_* &= \frac{2L_b\omega}{\sqrt{gh}} = \frac{2L_b}{L_g}, \quad \text{where} \quad L_g \equiv \frac{\sqrt{gh}}{\omega} \\
r_* &= \frac{r}{\omega h} = \frac{gU}{\omega h C^2} \\
b_* &= \frac{b_c+\Delta b}{b_c} \\
\Lambda_e &= b_* L_*^2 = \frac{b_c+\Delta b}{b_c}\frac{4L_b^2\omega^2}{gh} = \frac{4L_b^2\omega^2}{gA_c/b_{\text{tot}}}
\end{aligned} \tag{9}$$

Here we introduce the estuarine convergence number Λ_e, through which all geometrical and bathymetrical features of the rivers are accounted for. Λ_e decreases with increasing water depth and river convergence, and with loss of intertidal area. Note that the friction parameter $\widehat{\chi}$ introduced by Toffolon and Savenije (2011) is identical to r_*. Another important length scale is the friction length L_r, which follows from the non-linearized momentum equation $L_r = hC^2/g$.

Next, the quadratic dispersion Eq. 8 is resolved (using MAPLE), yielding the real and imaginary wave number for the tidal propagation in a converging estuary:

$$\kappa_r = \pm\frac{1}{2}\left[2\sqrt{(\Lambda_e-1)^2+(\Lambda_e r_*)^2}+2(\Lambda_e-1)\right]^{1/2} \tag{10a}$$

and

$$\kappa_i = 1\mp\frac{1}{2}\left[2\sqrt{(\Lambda_e-1)^2+(\Lambda_e r_*)^2}-2(\Lambda_e-1)\right]^{1/2} \tag{10b}$$

where the +/− sign represent the incoming wave in Eqs. 10a and 10b, respectively, and the −/+ sign the reflecting wave. This solution is identical to the solution presented by Jay (1991), Toffolon and Savenije (2011) and Van Rijn (2011). In Part II of this paper, it will become clear why we prefer the simple three parameter solution of Eq. 10.

Figure 6 shows the variation of the dimensionless real and imaginary wave number as a function of the estuarine convergence number Λ_e for two values of the dimensionless effective hydraulic drag $r_*=1$ and 6, characteristic for muddy and sandy beds, respectively. For low Λ_e and r_*, the tide becomes amplified, for sandy beds, characterized by larger roughness, not.

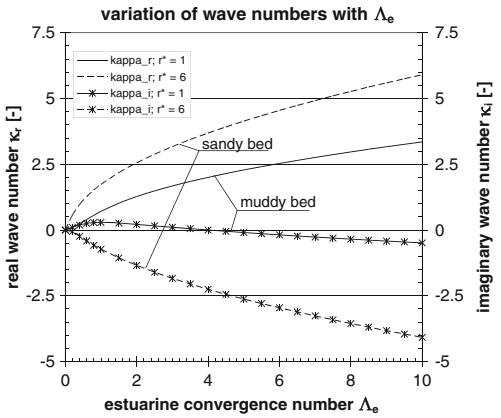

Fig. 6 Variation of dimensionless real and imaginary wave number with estuarine convergence number for incoming wave only (infinitely long estuary; e.g., Eqs. 10a and 10b)

Let us first analyze the behavior of these solutions for an infinitely long estuary. For a non-converging ($L_b=\infty$), frictionless channel ($r=0$), Eq. 10—in dimensional form—converges to the well-known relations $k_r = \omega\sqrt{(b_c+\Delta b)/b_c gh}$ and $k_i=0$. For a non-converging channel with friction, we obtain:

$$k_r = \pm\sqrt{\frac{b_*\omega^2}{2gh}}\left[\sqrt{1+r_*^2}+1\right]^{1/2} \quad \text{and} \quad k_i = \mp\sqrt{\frac{b_*\omega^2}{2gh}}\left[\sqrt{1+r_*^2}-1\right]^{1/2} \tag{11a}$$

Let us next analyze these solutions for a converging estuary with very high ($r=\infty$) and very low roughness ($r\approx 0$). In the first case the friction term dominates the expression below the square root-sign, in the second case, friction can be neglected. The real and imaginary wave number for a frictionless system read (assuming shallow water, i.e., h not too large)

$$\begin{aligned}
\kappa_r|_{r\downarrow 0} &= \sqrt{\Lambda_e-1} \quad \text{and} \quad \kappa_i|_{r\downarrow 0} = 1 \quad \text{for} \quad \Lambda_e \geq 1 \\
\kappa_r|_{r\downarrow 0} &= 0 \quad \text{and} \quad \kappa_i|_{r\downarrow 0} = 1-\sqrt{1-\Lambda_e} \quad \text{for} \quad \Lambda_e \geq 1
\end{aligned} \tag{11b}$$

Equation 11b shows that for a smooth bed and $\Lambda_e \geq 1$, the tidal wave is amplified with the convergence length $k_i = 1/2L_b$; this is therefore the maximum amplification of the tide according to linear theory; the estuary is said to be in synchronous mode (see below—weakly dissipative, Jay 1991; Lanzoni and Seminara 1998).

In case of a rough bed ($r=\infty$), the real and imaginary wave number become (strongly dissipative):

$$\begin{aligned}
k_r|_{r\uparrow\infty} &= \frac{1}{4L_b}\sqrt{2\Lambda_e r_*} \quad \text{or} \quad \kappa_r|_{r\uparrow\infty} = \sqrt{\Lambda_e r_*/2} \\
k_i|_{r\uparrow\infty} &= \frac{1}{2L_b}-\frac{1}{4L_b}\sqrt{2\Lambda_e r_*} \quad \text{or} \quad \kappa_i|_{r\uparrow\infty} = 1-\sqrt{\Lambda_e r_*/2}
\end{aligned} \tag{11c}$$

From Eq. 7, we can derive the velocity amplitude U_0 as a function of a_0:

$$U_0 = \mathrm{mod}\left[\frac{igka_0}{(i+r_*)\omega\exp\{-i\varphi\}}\right] = \frac{ga_0}{\omega}\sqrt{\frac{k_r^2+k_i^2}{r_*^2+1}} \tag{12}$$

The phase angle between tidal elevation and velocity follows from substitution of (6) into (5a), elaborating the real part only:

$$i\omega a_0 - i\frac{A_c}{b_c+\Delta b}kU_0\exp\{-i\varphi\} - \frac{A_c}{b_c+\Delta b}\frac{1}{L_b}U_0\exp\{-i\varphi\} = 0 \tag{5a'}$$

$$\tan\{\varphi\} = \frac{L_b k_i - 1}{L_b k_r} = \frac{\kappa_i - 2}{\kappa_r} \tag{13a}$$

Note the similarity of (13a) with Van Rijn's Table 1 (2011). Substituting from (11b and 11c) yields the phase angle for a smooth and friction-dominated system (see also Dronkers 2005 and Friedrichs 2010):

$$\begin{aligned}&\tan\{\varphi\}|_{r\downarrow 0} = -\frac{1}{\sqrt{\Lambda_e - 1}} \text{ for } \Lambda_e \geq 1 \text{ and } \tan\{\varphi\}|_{r\downarrow 0} = \infty;\ \varphi = 90^\circ \text{ for } \Lambda_e \leq 1\\ &\tan\{\varphi\}|_{r\uparrow\infty} = -\frac{\sqrt{\Lambda_e r_*}+2}{\sqrt{\Lambda_e r_*}} \approx -1 \text{ for all } \Lambda_e\end{aligned} \tag{13b}$$

The celerity c of the tidal wave into the estuary is given by:

$$c = \frac{\omega}{k_r} = \frac{2\omega L_b}{\kappa_r} \tag{14a}$$

Substituting from (11a) yields the celerity for a smooth and friction dominated system (e.g., Le Blond 1978):

$$\begin{aligned}c|_{r\downarrow 0} &= \frac{2\omega L_b}{\sqrt{\Lambda_e - 1}} \quad \text{for } \Lambda_e \geq 1 \text{ and } c|_{r\downarrow 0} = \infty \quad \text{for } \Lambda_e \leq 1\\ c|_{r\uparrow\infty} &= \frac{4\omega L_b}{\sqrt{2\Lambda_e r_*}} \quad \text{for all } \Lambda_e\end{aligned} \tag{14b}$$

The behavior of the tidal wave for frictionless conditions and $\Lambda_e \leq 1$ (i.e., $L_b \leq L_g/2$ for $\Delta b = 0$) needs some further explanation. For these conditions, the wave length and celerity become infinite, whereas the phase angle between water level and velocity becomes 90°. Though these conditions are identical to those of a standing wave, we have to realize we did not prescribe any wave reflections in our boundary conditions. Though this pathological behavior is referred to as super-critical by Toffolon and Saveneije (2011), and was also found by Friedrichs and Aubrey (1994), we do not really understand the physical meaning of these solutions to the equations, and the conditions at which these occur.

Next, we study the propagation and amplification/damping of the tide in an estuary of finite length ℓ (for instance by a weir at $x = \ell$). At the mouth of the estuary we prescribe a simple cosine tide:

$$\eta(0,t) = h + a_0\cos\{\omega t\} \tag{15}$$

in which a_0=amplitude of the tide in the river mouth. The harmonic solution to Eq. 5 than reads:

$$\begin{aligned}\eta(x,t) &= h + a_0^+\exp\{i(\omega t - k^+x)\} + a_0^-\exp\{i(\omega t - k^-x)\} \text{ and}\\ u(x,t) &= U_0^+\exp\{i(\omega t - k^+x - \varphi)\} + U_0^-\exp\{i(\omega t - k^-x - \varphi)\}\end{aligned} \tag{16a}$$

in which the superscripts $\cdot^+$ and $\cdot^-$ reflect the incoming and reflecting tidal wave. In case of an infinitely long river, Eq. 16a reduces to:

$$\eta(x,t) = h + a_0\exp\{i(\omega t - kx)\} \quad \text{and} \quad u(x,t) = U_0\exp\{i(\omega t - kx - \varphi)\} \tag{16b}$$

as in Eq. 6. The boundary conditions to the solution of Eq. 16a are given by:

- $x = 0$: $a_0^+ + a_0^- = a_0$; this conditions implies that in the analyses of Part II, for rivers with a weir, the river should be so long (friction length small) that $a_0 = a_0^+$,
- $x = \ell$: $U = 0$, hence $U^+ = -U^-$.
  Further to Eq. 5b, the latter implies that
- $x = \ell : \partial a^+/\partial x = -\partial a^-/\partial x$, so that
  $a_0^+ k^+\exp\{-ik^+\ell\} + a_0^- k^-\exp\{-ik^-\ell\} = 0$.

Hence, we find for the two complex amplitudes of the incoming and reflecting waves a^+ and a^-:

$$a^+ = \frac{k^-\exp\{-ik^-\ell\}\exp\{-ik^+x\}}{k^-\exp\{-ik^-\ell\} - k^+\exp\{-ik^+\ell\}}a_0 \tag{17a}$$

$$a^- = \frac{k^-\exp\{-ik^+\ell\}\exp\{-ik^-x\}}{k^+\exp\{-ik^+\ell\} - k^-\exp\{-ik^-\ell\}}a_0 \tag{17b}$$

As $k^- = -k_r + ik_i^- = -k_r + i(p+q)$ and $k^+ = k_r + ik_i^+ = k_r + i(p-q)$, where p and q are dummy variables (see Eq. 10), we can re-write (17) as:

$$a_0^+ = \frac{k^-\exp\{ik_r\ell\}}{k^-\exp\{ik_r\ell\} - k^+\exp\{-ik_r\ell\}\exp\{-2q\ell\}}a_0 \tag{18a}$$

$$a_0^- = \frac{k^+\exp\{-ik_r\ell\}\exp\{-2q\ell\}}{k^+\exp\{-ik_r\ell\}\exp\{-2q\ell\} - k^-\exp\{ik_r\ell\}}a_0 \tag{18b}$$

Hence, $\lim_{\ell\to\infty}\{a_0^+\}=a_0$ and $\lim_{\ell\to\infty}\{a_0^-\}=0$, retrieving the simple propagating wave in an infinitely long converging estuary. Furthermore, Eq. 17 shows that resonance can occur when:

$$\mathrm{Re}[k^+\exp\{-ik^+\ell\}-k^-\exp\{-ik^-\ell\}]=0,\ \text{i.e.,}\quad \tan\left\{n\frac{\pi}{2}-k_r^+\ell\right\}=\frac{k_r^+\exp\{k_i^-\ell\}+k_r^+\exp\{k_i^+\ell\}}{k_i^+\exp\{k_i^+\ell\}+k_i^-\exp\{k_i^-\ell\}} \tag{19}$$

As Eq. 19 is implicit in ℓ, we cannot determine the conditions for resonance analytically. However, for a straight channel, $k_i^-=-k_i^+$ (e.g., Eq. 10b), $\tan\{k_r\ell\}=\infty$, which is the case if $\ell=\lambda/4$, where λ=wave length in a straight frictionless channel, e.g., Dronkers (1964). For a very strong converging channel, e.g., $\lim_{L_b\to0}k_r=\lim_{L_b\to0}k_i^+=\lim_{L_b\to0}k_i^-=1$, $\tan\{k_r\ell\}=1$, and $\ell=\lambda/8$. Of course, the wave length in a straight and very converging channel are very much different (in fact if $L_b=0$, $\lambda=0$).

The solution to Eq. 19 is depicted graphically in Fig. 7 (see also Prandle and Rahman (1980)). Note that typical values for Λ_e range from a bit smaller than 1 to about 2 (e.g., Part II). The effect of reflections will grow rapidly with decreasing effective hydraulic roughness, as both the tidal amplitude and friction length will than increase.

Next, we study the dependency of tidal asymmetry on the estuarine bathymetry. Though we prescribe harmonic solutions in a linear model (Eqs. 5 and 16a with one frequency only), we can derive a proxy for the tidal asymmetry by analyzing the celerity of the tidal wave. In the following, we limit ourselves to infinitely long channels only. Further to Friedrichs (2010) and Dronkers (2005), we define an asymmetry parameter $\gamma=c_{\mathrm{HW}}/c_{\mathrm{LW}}$, where c_{HW} and c_{LW} are the celerity at high water (i.e., $h=h_0+a$) and low water (i.e., $h=h_0-a$), respectively:

$$\gamma=\frac{k_{r,\mathrm{LW}}}{k_{r,\mathrm{HW}}}=\left[\frac{(1+a/h)}{(1-a/h)}\right]^{1/2}\left[\frac{\left[\sqrt{\left(L_*^2-(1-a/h)\right)^2+\left(\frac{L_*^2r_*}{(1-a/h)}\right)^2}+\left(L_*^2-(1-a/h)\right)\right]}{\left[\sqrt{\left(b_*L_*^2-(1+a/h)\right)^2+\left(\frac{b_*L_*^2r_*}{(1+a/h)}\right)^2}+\left(b_*L_*^2-(1+a/h)\right)\right]}\right]^{1/2} \tag{20}$$

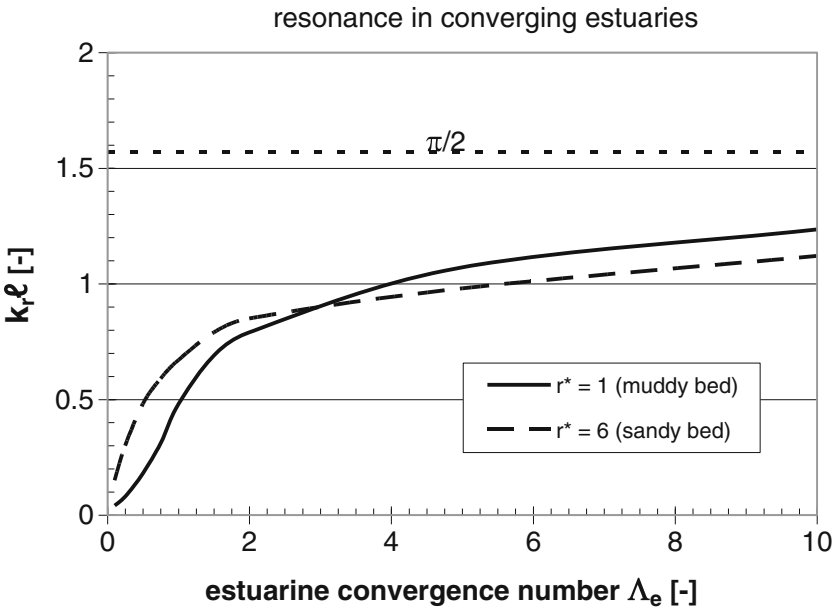

Fig. 7 Conditions for resonance (solution of Eq. 19) for a converging estuary as a function of the estuarine convergence number

in which we assume that $\Delta b=0$ at low water, and the dimensionless parameters have been defined in Eq. 9. Note that this proxy is relevant for progressive waves only, and loses its meaning in case of a truly standing wave. Further, for a friction-dominated system we find:

$$\gamma|_{r=\infty}=\left.\frac{k_{r,\mathrm{LW}}}{k_{r,\mathrm{HW}}}\right|_{r=\infty}\approx\left[\frac{\frac{1}{(1-a/h)}\,\frac{1}{(1-a/h)}}{\frac{b_*}{(1+a/h)}\,\frac{1}{(1+a/h)}}\right]^{1/2}=\frac{1+a/h}{1-a/h}\sqrt{\frac{1}{b_*}}\approx\frac{(1+a/h)^2}{\sqrt{b_*}} \tag{21a}$$

Of course, this solution can be derived directly from the general formulation of wave celerity in a straight prismatic compound channel, e.g., $c=\sqrt{gA_c/b_{\mathrm{tot}}}$. For a frictionless system we find four solutions, depending whether L_*^2 and $b_*L_*^2$ are larger or smaller than $(1-a/h)$ or $(1+a/h)$, respectively. We give one solution:

$$\gamma|_{r=0}=\left.\frac{k_{r,\mathrm{LW}}}{k_{r,\mathrm{HW}}}\right|_{r=0}\approx\left[\frac{(1+a/h)^2\Lambda_e/b_*-(1+a/h)}{\Lambda_e-(1+a/h)}\right]^{1/2}\quad\text{for}\quad L_*^2\geq(1-a/h)\ \text{ and }\ b_*L_*^2\geq(1+a/h) \tag{21b}$$

In the next section, we study the behavior of these solutions graphically, analyzing the response of an estuary to deepening and narrowing (loosing intertidal area).

5 Conceptual response to narrowing and deepening

In Part II of this paper, we analyze the historical evolution of four rivers, e.g., the Elbe, Ems, Loire, and Scheldt Rivers. The length of Ems and Scheldt is restricted by a weir (at Herbrum and Ghent, respectively), hence the tide is likely to be affected by reflections. The depth of the Elbe changes so abruptly beyond Hamburg, that also in the Elbe tidal reflections are to be expected. Hence, ideally, we should use the full analytical solution (Eq. 17) to study the tidal properties in these rivers. However, this is not easy, as the depth along these rivers varies considerably, and also the convergence length of two rivers (Elbe and Scheldt) is not constant. Modeling the tide in such inhomogeneous rivers requires division of the river into sub-sections. This is indeed done in Part II. From a mathematical point of view, accounting for reflections of the tide requires internal boundary conditions between the various sub-sections. This has been elaborated by, e.g., Prandle and Rahman (1980), Jay (1991), and Toffolon and Savenije (2011). However, the extensive set of equations lose their clarity, while this clarity was the major reason for developing the current new approach. Therefore, in Part II we analyze these four rivers, assuming infinite length, and we discuss the behavior of the solutions of the previous section for infinitely long rivers as well.

Yet, for the Elbe, Ems, and Scheldt, we assess the effects of tidal reflections in a qualitative way, and in the following, we elaborate briefly the behavior of the full solution (Eq. 17) by studying that solution graphically. First, we analyze the conditions for resonance in an almost straight channel of 5 m depth, and a weir at 75 km (about 1/4 of the undisturbed tidal wave length), as discussed by Dronkers (1964). The results are presented in Fig. 8 for three different friction coefficients; these results are indeed identical to those found by Dronkers (1964). As mentioned, tidal amplification by reflections is expected to grow rapidly with increasing SPM concentrations, as tidal amplitude and friction length both increase with decreasing hydraulic drag.

Next, we study the effect of river convergence. Figure 9 presents the computed tidal amplitudes in a 5-m deep converging river (L_b=33 km, e.g., Ems conditions) with and without a weir for two values of the friction coefficient, the smaller representative for high SPM conditions and the larger

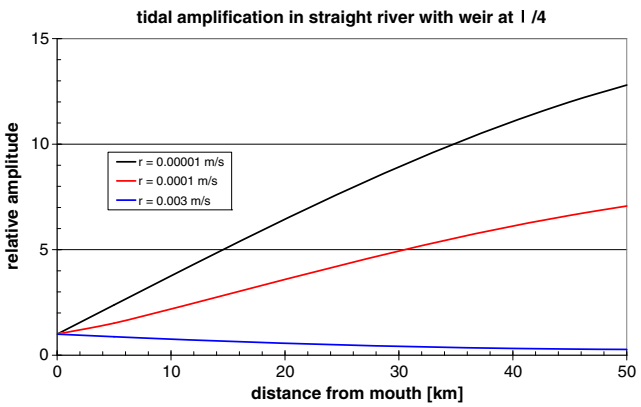

Fig. 8 Amplification of tidal wave in 5 m deep, almost straight estuary (L_b=50,000 km, λ=350 km) and weir at ℓ =75 km; r=0.000001 m/s yields $C\approx$1,000 m$^{1/2}$/s (e.g., almost frictionless); r=0.0001 m/s yields $C\approx$300 m$^{1/2}$/s and r=0.003 yields C≈60 m$^{1/2}$/s

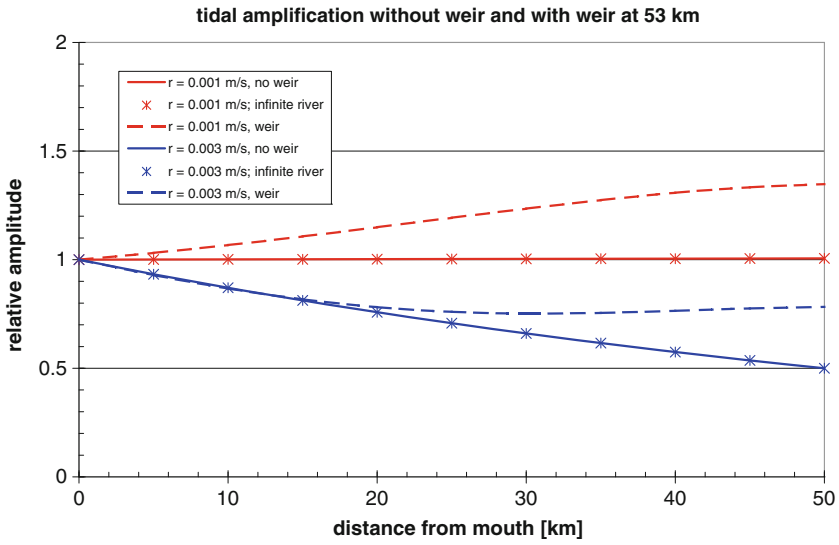

Fig. 9 Amplification of tidal wave in short converging estuary (h=5 m, L_b=33 km, ℓ =53 km); r=0.001 m/s yields $C \approx 100$ m$^{1/2}$/s; r=0.003 yields $C \approx 60$ m$^{1/2}$/s

for low SPM concentrations. Though the increase in tidal amplitude is not too different for both cases, the tide in the sandy system remains damped, whereas in the muddy system, the tide becomes amplified.

To check our full solution (e.g., with reflections), we have also plotted the imaginary wave number (10b), which gives directly the relative amplitude in an infinitely long channel, showing exact overlap with Eq. 17 for $\ell = \infty$.

In the last part of this section, we discuss the behavior of the solutions of the previous section for an infinitely long channel, assuming a convergence length of 33 km, throughout. Figure 10 presents the phase difference between the flow velocity and tidal elevation φ (e.g., Eq. 13a) as a function of depth, width of intertidal area, and bed friction. Figure 11 presents the celerity c of the tidal wave into the estuary, using Eq. 14a. Because of the rapid increase in c with depth h and inverse friction $1/r$, we have used a logarithmic axis.

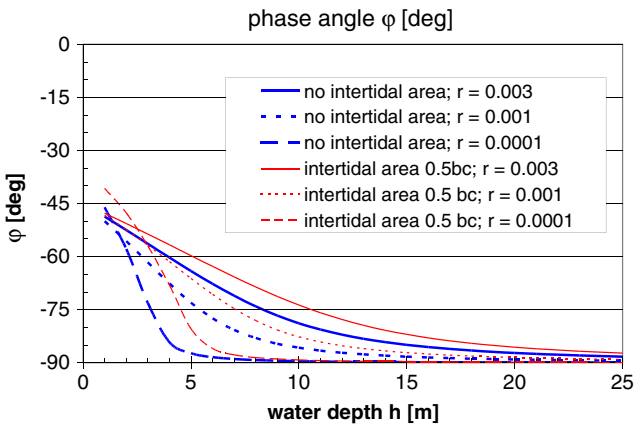

Fig. 10 Phase angle φ between flow velocity and tidal elevation ($\ell = \infty$, L_b=33 km)

For φ=90° (e.g., Fig. 10), high water slack (HWS) occurs at high water (HW), as for standing waves. This condition is met at large water depths, but also at moderate water depths when the hydraulic drag becomes very small. The latter is the case in the presence of pronounced concentration of SPM (several 10 g/l), as in the Ems and Loire Rivers. Figure 10 shows that c then increases rapidly, and can become so large that high waters along the estuary occur almost simultaneously. For instance, for h=7 m, and r=0.001, we find c=100 m/s (e.g., Fig. 11), and high water at 60 km from the river mouth would occur only 10 min after high water at that mouth. Note that a "normal" progressive wave approach $c = \sqrt{gh}$ would yield a travel time of almost 2 h.

From Eq. 5a we assess that φ=90° occurs when $\partial u/\partial x$=0 (see also Dronkers 2005 and Friedrichs 2010), and from Eq. 13a, we conclude that φ=90° implies k_r=0. The latter is true only for a real standing wave, which implies resonant behavior in the estuary. Note that this solution still represents a progressive wave, even when reflections become important. The first observation also implies large flow velocities over the major part of the estuary. Then, owing to the harmonic solution prescribed (Eq. 6), also the tidal amplitude is more or less constant over a large part of the estuary. An estuary with such conditions is called synchronous (e.g., Dronkers 2005). Examples are the current conditions in the Ems and Loire River (e.g., Part II).

Note that the evolution towards a synchronous estuary is delayed in case of presence of (some) intertidal area, e.g., Fig. 10. However, the celerity decrease with $\Delta b/b_c$ (results not shown), though is not too sensitive to the intertidal area.

Next, we study the conceptual character of the tidal properties in a tidal river in response to deepening as a function of the areal of intertidal area and the effective hydraulic drag, simulating low (r=0.003 m/s; $C \approx 60$ m$^{1/2}$/s) and high SPM concentrations (r=0.001 m/s, $C \approx 100$ m$^{1/2}$/s).

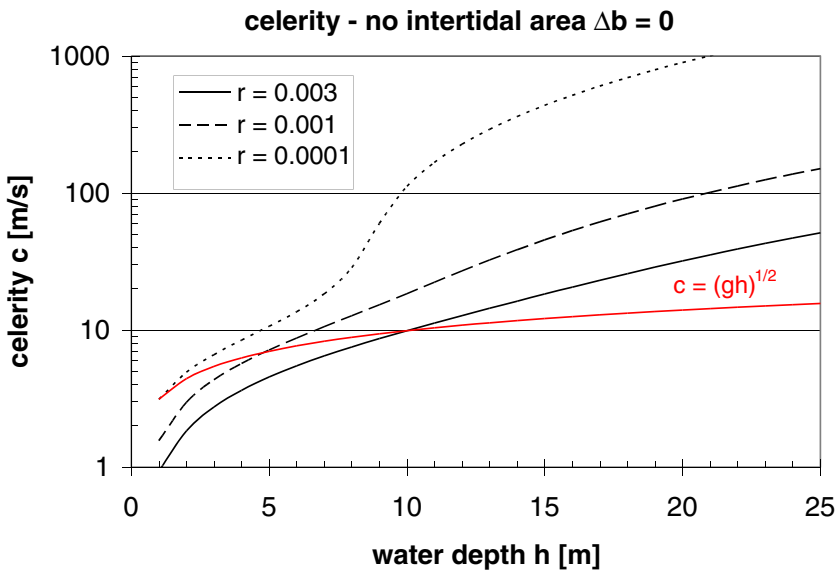

Fig. 11 Celerity of tidal wave ($\ell=\infty$, L_b=33 km)

The convergence length is set again at 33 km, and we prescribe a tidal amplitude in the mouth of the river of 1 m to depict the tidal response clearly, though this amplitude is possibly a bit high with respect to our linear assumptions. The intertidal area is set at $\Delta b = b_c$ or $\Delta b = 0$.

First we discuss the situation with low SPM concentrations (r=0.003 m/s). Figure 11 shows that when the river is deepened, the tidal amplitude increases, as expected. Without intertidal area, the response is a bit stiffer. For large water depth, the amplitude for the case with intertidal area is a bit larger than in the case without intertidal, as in the first case more water enters the river.

Figure 13 shows that the proxy for tidal asymmetry γ changes from ebb dominance for all water depths to flood-dominant conditions in case the intertidal area is removed. This observation is not new of course (e.g., Friedrichs and Aubrey 1988), but the implications for fine sediments have not been elaborated. When the tidal river becomes flood dominant, marine fine sediments are pumped into the river and/or riverine fine sediment are kept within the river. Then, if sufficient fines have accumulated, and are distributed over a considerable length of the river, the effective hydraulic drag is expected to decrease (e.g., Section 3 of this paper). In response to this lower drag (simulated with r=0.001 m/s), amplification increases further, as depicted in Fig. 12, accompanied by an enhancement of flood dominance, e.g., Fig. 13. As a result, more fines can accumulate in the river, further decreasing the effective hydraulic drag, setting in motion the snowball effect suggested in the beginning of this paper.

The next section discusses some implications of this picture, and in Part II we analyze historical data to study whether this feed-back can be observed in European rivers.

6 Discussion, summary, and conclusions

This paper presents a conceptual picture on the evolution of a number of "normal" European tidal rivers into a hyper-turbid state in response to narrowing and deepening accommodating ever-larger ships. Part II of this paper describes the actual analysis of the historical data of four European rivers, e.g., the Elbe, Ems, Loire, and Scheldt rivers. In the current Part I,

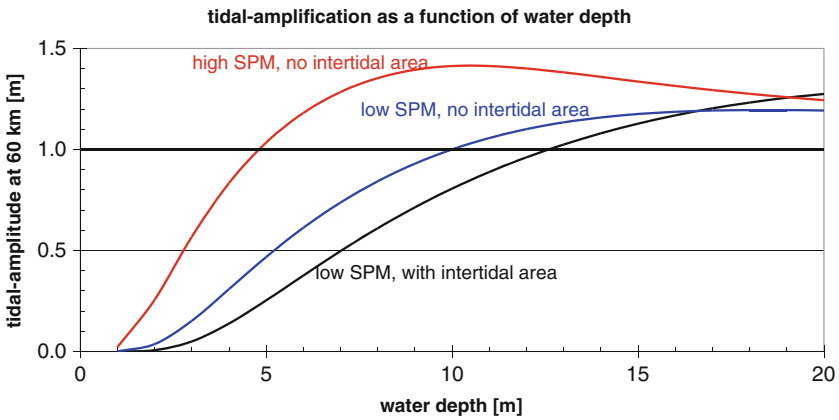

Fig. 12 Response of tidal amplification as a function of water depth, intertidal area, and effective hydraulic drag

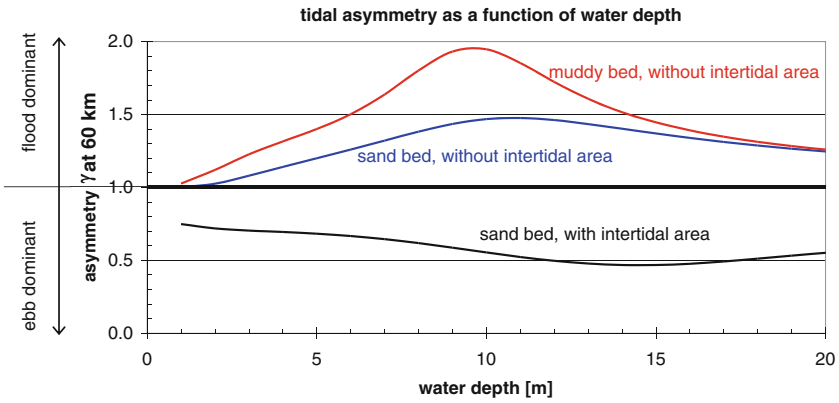

Fig. 13 Response of tidal asymmetry as a function of water depth, intertidal area, and effective hydraulic drag

the ingredients required for the analysis and interpretation of the data in Part II are derived and summarized. Our main tool in this is the analytical solution of the linearized water movement equations. Though not new, the solution is formulated in a form that can be used easily to compare the evolution of the various rivers.

Our analysis of the analytical solution itself suggests that, after loss of intertidal area, ongoing deepening may enhance flood dominancy, while decreasing the river's flushing capacity. As discussed in Part II, loss of intertidal area has been considerably in the nineteenth century, reclaiming intertidal areas and embanking rivers. Thus, conditions may be induced favorable for the generation of a secondary turbidity maximum, referred to as ETM2. Then, if large amounts of fine sediments would accumulate in the river, the effective hydraulic drag decreases, enhancing the tidal asymmetry further. It is noted that this feed-back may occur already at SPM concentrations of several 100 mg/l (Winterwerp et al. 2009). However, the suspended matter should be spread over a considerable length of the river to induce a measurable reduction in drag. As the accumulation of fines takes time, the time-scale for a regime shift towards hyper-turbid conditions is expected to take considerable time after "favorable" conditions for such a regime shift have been established (the tipping point). When SPM concentrations

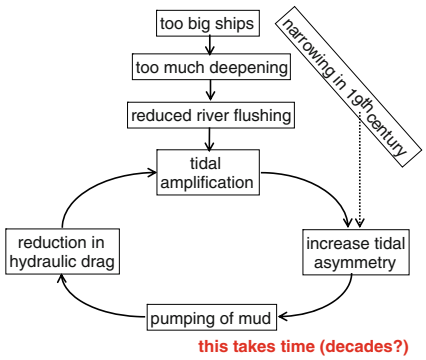

Fig. 14 Conceptual positive feedback loop inducing hyper-concentrated conditions in tidal rivers after intertidal area has been lost, which happened for many rivers in the late nineteenth century

continue to increase, entrainment processes re-fluidize the mud every accelerating tide, preventing consolidation of the sediment–water mixture. Thus, the ETM2 conditions become self-maintaining, as the hyper-turbid state is favorable from an energy point of view as well (e.g., Section 2). These ETM2 conditions can therefore be considered as an alternative state in relation to the ETM1 state, common in most "normal" estuaries. This positive feed-back loop is sketched in Fig. 14, depicting the proposed snowball effect leading to hyper-turbid conditions.

As high SPM concentrations in the water column are a necessary condition for the feed-back between tidal amplification and reduction in hydraulic drag, accommodation of fines on intertidal areas may prevent a regime shift in tidal rivers. Thus, intertidal area has two functions:

- With sufficient intertidal area, tidal conditions remain ebb-dominant, preventing the formation of ETM2 conditions. However, a considerable intertidal area is required, estimated at least 50 % of the width of the flow-carrying cross-section (see also Friedrichs and Aubrey 1988).
- Intertidal area can however also accommodate large amounts of fine sediments, preventing their accumulation in the water column. The area required to prevent a regime shift towards hyper-turbid conditions is site-specific, but likely much smaller than the intertidal areas required to affect tidal asymmetry.

It is finally noted that in the current paper three important effects are not being treated (in detail):

- The tidal evolution may be affected by the construction of a weir, limiting the effective length of the river. The reflections of the tidal wave are felt over increasing lengths of the estuary when the effective hydraulic drag decreases. The underlying increase in roughness length is not only the result of a decrease in friction coefficient, but also by the increase in the celerity of the tidal wave.
- Tidal asymmetry in an estuary is not only generated internally, but may also be "imported" from the estuaries

environment, for instance a shallow sea in which the estuary flows (e.g., Schuttelaars et al. 2012).
- The effect of river flow with respect to flushing has been discussed (though not quantified); however, river flows can affect the tidal propagation as well, which cannot be elaborated with the linear model in this paper.

In a next phase of this study, we will address these issues, and other non-linear effects with a numerical model, operated in the same sense as the analytical model of this paper, as elaborated upon in Part II of this paper.

Acknowledgments This work was carried within the framework of the LTV project, which is the acronym for Long-Term Vision of Scheldt estuary with respect to Safety, Accessibility, and Nature, in which the following sub-projects are integrated: Maintaining fairways Scheldt estuary, Permits for disposal of dredged sediments, and the so-called KPP (knowledge of primary processes) program of Rijkswaterstaat. The study was financed by the Flemish "Afdeling Maritieme Toegang" (Maritime Department) and Rijkswaterstaat, Waterdienst, and Directorate Zeeland (the Dutch Ministry of Infrastructure and Environment). The subject of the research in this paper was formulated by Mr. Youri Meersschaut requesting the analysis of the fine sediment dynamics in the Scheldt River. Further, we like to thank Mr. Cees Kuijper and Dr. Henk Schuttelaars for their many constructive comments and ongoing discussions on this subject, and Dr. Tom de Mulder for reviewing a report of this study. We also would like to acknowledge the help of Mr. Marcel Taal in organizing and coordinating our study.

References

Brenon I, LeHir P (1999) Modeling the turbidity maximum in the seine estuary (France): identification of formation processes. Estuar Coast Shelf Sci 49:525–544

Bruens AW, Winterwerp JC, Kranenburg C (2012) Physical and numerical modeling of the entrainment by a high-concentrated mud suspension. J Hydraul Eng ASCE 138(6):479–490. doi:10.1061/(ASCE)HY.1943-7900.0000545

Cai H, Savenije HHG, Toffolon M (2012) A new analytical framework for assessing the effects of sea-level rise and dredging on tidal damping in estuaries. J Geophys Res 117: C09023. doi:10.1029/2012JC008000

Chernetsky AS, Schuttelaars HM, Talke SA (2010) The effect of tidal asymmetry and temporal settling lag on sediment trapping in tidal estuaries. Ocean Dyn 60:1219–1241. doi:10.1007/s10236-010-0329-8

Dankers PJT, Winterwerp JC (2007) Hindered settling of mud flocs: theory and validation. Cont Shelf Res 27:1893–1907

Dronkers JJ (1964) Tidal computations in river and coastal waters. Elsevier, New York

Dronkers J (2005) Dynamics of coastal systems. Advanced Series on Ocean Engineering—Vol 25. World Scientific

Dyer KR (1997) Estuaries: a physical introduction. Wiley, Chichester

Friedrichs CT, Aubrey DG (1988) Non-linear tidal distortion in shallow well-mixed estuaries: a synthesis. Estuar Coast Shelf Sci 27:521–545

Friedrichs CT, Aubrey DG (1994) Tidal propagation in strongly convergent channels. J Geophys Res 99:3321–3336

Friedrichs CT (2010) Barotropic tides in channelized estuaries. In: Valle-Levinson A (ed) Contemporary issues in estuarine physics. Cambridge University Press, Cambridge, pp 27–61

Hunt JN (1964) Tidal oscillations in estuaries. Geophys J R Astron Soc 8: 440–455

Jay DA (1991) Green law revisited: tidal long-wave propagation in channels with strong topography. J Geophys Res 96(C11):20,585–20,598

Jay DA, Musiak JD (1996) Internal tide asymmetry in channels: origins and consequences. In: Pattiaratchi C (ed) Mixing processes in estuaries and coastal seas. Am Geophys Union Coast Estuar Sci Monogr 219-258

Lanzoni S, Seminara G (1998) On tide propagation in convergent estuaries. J Geophys Res 103(C13):30,793–30,812

LeBlond PH (1978) On tidal propagation in shallow rivers. J Geophys Res 83:4717–4721

Lin J, Kuo AY (2001) Downstream turbidity maximum in the York River, Virginia. Estuaries 24:707–720

Prandle D, Rahman M (1980) Tidal response in estuaries. J Phys Oceanogr 10:1552–1573

Savenije HHG (2001) A simple analytical expression to describe tidal damping or amplification. J Hydrol 243(3–4):205–215

Schuttelaars HM, de Jonge VN, Chernetsky A (2012) Improving the predictive power when modeling physical effects of human interventions in estuarine systems. Ocean Coast Manage. doi:10.1016/j.ocecoaman.2012.05.009

Soulsby RL, Wainwright BLSA (1987) A criterion for the effect of suspended sediment on near-bottom velocity profiles. J Hydraul Res 25(3):341–356

Speer PE, Aubrey D (1985) A study of non-linear tidal propagation in shallow inlet/estuarine systems I, Theory. Estuar Coast Shelf Sci 21: 206–240

Talke SA, de Swart HE, Schuttelaars HM (2008) An analytical model for the equilibrium distribution of sediment in an estuary. In: Dohmen-Janssen CM, Hulscher SJMH (eds) River, coastal and estuarine morphodynamics. Taylor & Francis, London, pp 403–412

Talke SA, de Swart HE, Schuttelaars HM (2009) Feedback between residual circulations and sediment distribution in highly turbid estuaries: an analytical model. Cont Shelf Res 29:119–135. doi:10.1016/j.csr.2007.09.002

Taylor PA, Dyer KR (1977) Theoretical models of flow near the bed and their implications for sediment transport. The Sea 6:579–601

Toffolon M, Vignoli G, Tubino M (2006) Relevant parameters and finite amplitude effects in estuarine hydrodynamics. J Geophys Res 111: C10014. doi:10.1029/2005JC003104

Toffolon M, Savenije HG (2011) Revisiting linearized one-dimensional tidal propagation. J Geophys Res 116: C07007. doi:10.1029/2010JC006616

Turner JS (1973) Buoyancy effects in fluids. Cambridge University Press

Vanoni VA (1946) Transportation of suspended sediment by water. ASCE Trans 111(2267):67–133

Van Rijn LC (1993) Principles of sediment transport in rivers, estuaries and coastal seas, AQUA Publications, The Netherlands.

Van Rijn LC (2011) Analytical and numerical analysis of tides and salinities in estuaries; part I: tidal wave propagation in convergent estuaries. Ocean Dyn 61:1719–1741. doi:10.1007/s10236-011-0453-0

Villaret C, Trowbridge JH (1991) Effects of stratification by suspended sediments on turbulent shear flows. J Geophys Res 96(C6):10659–10680

Winterwerp JC (2001) Stratification of mud suspensions by buoyancy and flocculation effects. J Geophys Res 106(10):22,559–22,574

Winterwerp JC, Lely M, He Q (2009) Sediment-induced buoyancy destruction and drag reduction in estuaries. Ocean Dyn 59(5):781–791

Winterwerp JC (2006) Stratification effects by fine suspended sediment at low, medium and very high concentrations. Geophys Res 11(C05012):1–11

Winterwerp JC (2011) Fine sediment transport by tidal asymmetry in the high-concentrated Ems River. Ocean Dyn 61(2–3):203–216. doi:10.1007/s10236-010-0332-0